OPEN

NPG Asia Materials (2016) 8, e321; doi:10.1038/am.2016.157
www.nature.com/am

ORIGINAL ARTICLE

Monolayer 1*T*-$NbSe_2$ as a Mott insulator

Yuki Nakata[1], Katsuaki Sugawara[2], Ryota Shimizu[2,3], Yoshinori Okada[2], Patrick Han[2], Taro Hitosugi[2,3], Keiji Ueno[4], Takafumi Sato[1] and Takashi Takahashi[1,2]

The emergence of exotic quantum phenomena is often triggered by a subtle change in the crystal phase. Transition metal dichalcogenides (TMDs) exhibit a wide variety of novel properties, depending on their crystal phases, which can be trigonal prismatic (2*H*) or octahedral (1*T*). Bulk $NbSe_2$ crystallizes into the 2*H* phase, and the charge density wave and the superconductivity emerge simultaneously and interact with each other, thereby creating various anomalous properties. However, these properties and their interplay in another polymorph, 1*T*-$NbSe_2$, have remained unclear because of the difficulty of synthesizing it. Here we report the first experimental realization of a monolayer 1*T*-$NbSe_2$ crystal grown epitaxially on bilayer graphene. In contrast with 2*H*-$NbSe_2$, monolayer 1*T*-$NbSe_2$ was found to be a Mott insulator, with an energy gap of 0.4 eV. We also found that the insulating 1*T* and metallic 2*H* phases can be selectively fabricated by simply controlling the substrate temperature during epitaxy. The present results open a path to crystal-phase engineering based on TMDs.
NPG Asia Materials (2016) **8,** e321; doi:10.1038/am.2016.157; published online 4 November 2016

INTRODUCTION

Atomic-layer materials have recently attracted attention, because they exhibit a variety of anomalous properties distinct from those of their three-dimensional bulk counterparts, as exemplified by the Dirac-cone states in graphene[1] and the high-temperature superconductivity in ultrathin iron-based superconductor films.[2] Whereas atomic-layer materials are inherently unstable, owing to their tendency to progress toward long-range order,[3] such characteristics may facilitate the exploration of new crystal phases that cannot usually be realized in bulk. For instance, the local crystal structure at the surfaces of transition metal dichalcogenides (TMDs) is known to be sensitive to crystal defects, chemical reactions and thermal effects,[4–9] thus suggesting the feasibility of crystal-phase control in two dimension. The structural transition between 2*H*- (trigonal prismatic structure, D_{3h}) and 1*T*- (octahedral structure, O_h) polymorphs (see Figure 1a) in monolayer MoS_2 is a typical example that cannot be achieved in the bulk phase.[5–7] Bulk $NbSe_2$ has several polymorphs: 3*R*, 4*H* and 2*H*, although the essential structural unit is identical, trigonal prismatic. Here we term a monolayer consisting of this structural unit 2*H*-$NbSe_2$.

Among TMDs, bulk 2*H*-$NbSe_2$ has been the target of intensive studies, because it exhibits a unique ground state in which an incommensurate charge density wave (CDW) and superconductivity coexist below 7 K.[10] Recent success in fabricating monolayer and multilayer 2*H*-$NbSe_2$ films has revealed drastic changes in the superconducting and CDW transition temperatures with changes in the number of layers, thus providing a valuable opportunity for studying key questions regarding the interplay among dimensionality, the CDW and superconductivity.[11–14] In contrast to the intensively studied 2*H*-$NbSe_2$,[15,16] the 1*T* counterpart has not yet been synthesized either in bulk or as an ultrathin film. Although a 1*T*-like phase has been observed locally around defects[17–19] in thermally treated bulk samples,[20] $Ag_xNb_2Se_3$ (Koslowski *et al.*[21]) and $Nb_{1-x}Ti_xSe_2$ (Di Salvo *et al.*[22]), it has been difficult to selectively fabricate a pristine sample of a single phase for precise physical measurements as well as for device applications. It is thus of great importance to fabricate an ultrathin film of pristine 1*T*-$NbSe_2$ and to investigate its electronic states to reveal as-yet-unknown electronic properties. Here, combining molecular-beam epitaxy and state-of-the-art electron spectroscopy methods, we succeeded in selectively fabricating 1*T* and 2*H* single-phase monolayer $NbSe_2$ on bilayer graphene and investigated the anomalous electronic states in detail.

MATERIALS AND METHODS

A monolayer $NbSe_2$ film was grown on bilayer graphene by using molecular-beam epitaxy in ultrahigh vacuum (3×10^{-10} Torr). Bilayer graphene was prepared by annealing an *n*-type Si-rich 6*H*-SiC(0001) single-crystal wafer,[23,24] by resistive heating at 1100 °C in high vacuum—better than 1.0×10^{-9} Torr—for 20 min. A monolayer $NbSe_2$ film was grown by evaporating Nb on the bilayer graphene substrate in a Se atmosphere. The substrate was kept at 500–590 °C during epitaxy. The as-grown film was annealed at 400 °C for 30 min and then transferred to the angle-resolved photoemission spectroscopy (ARPES)-measurement chamber without breaking vacuum. The growth process was monitored by reflection high-energy electron diffraction. The custom-made scanning tunneling microscopy (STM) system was operated at $T=4$–6 K under ultrahigh vacuum (below 2×10^{-10} Torr). The ARPES measurements were carried out using an MBS-A1 (MB Scientific AB, Uppsala, Sweden) electron-energy analyzer with a high-flux helium discharge lamp and a toroidal grating monochromator at Tohoku University. The energy and angular resolutions were set at 16 meV and 0.2°, respectively. The Fermi level (E_F) of

[1]Department of Physics, Tohoku University, Sendai, Japan; [2]WPI Research Center, Advanced Institute for Materials Research, Tohoku University, Sendai, Japan; [3]Department of Applied Chemistry, Tokyo Institute of Technology, Tokyo, Japan and [4]Department of Chemistry, Graduate School of Science and Engineering, Saitama University, Saitama, Japan
Correspondence: Dr K Sugawara, WPI Research Center, Advanced Institute for Materials Research, Tohoku University, Katahira 2-1-1, Aoba-ku, Miyagi, Sendai 980-8577, Japan.
E-mail: k.sugawara@arpes.phys.tohoku.ac.jp
Received 13 May 2016; revised 29 July 2016; accepted 20 August 2016

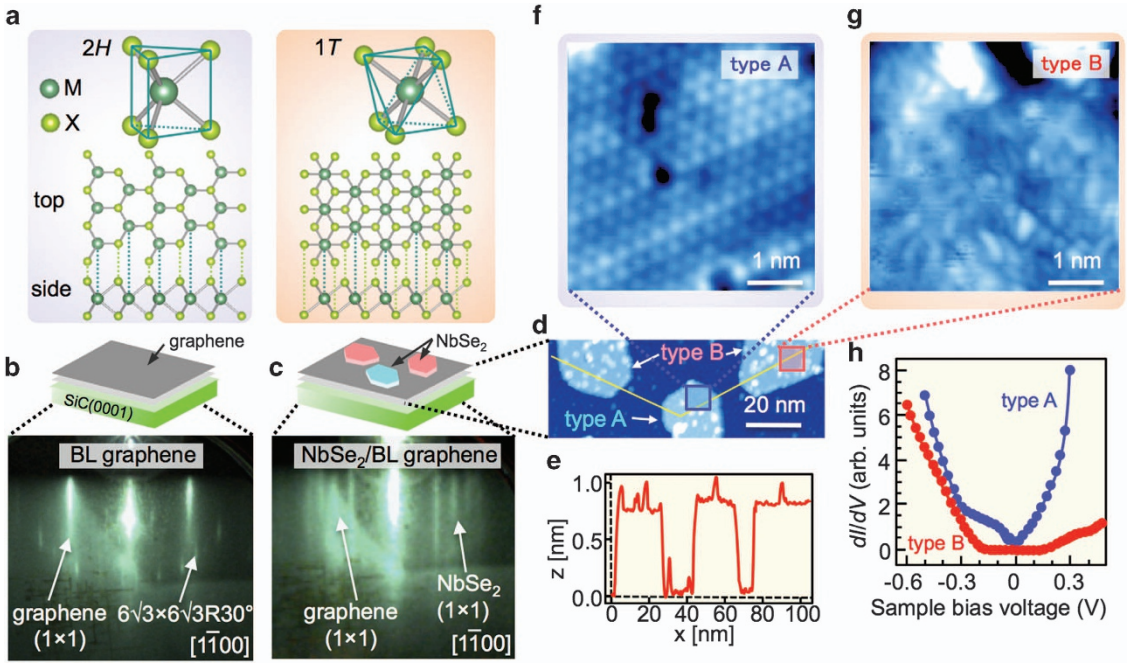

Figure 1 Characterization of monolayer 2*H*- and 1 *T*-$NbSe_2$. (**a**) Schematic crystal structure of monolayer 2*H*- and 1*T*-MX_2 (*M*=transition metal; *X*=chalcogen), shown in top and side views. (**b**, **c**) Reflection high-energy electron diffraction (RHEED) patterns of bilayer (BL) graphene and monolayer $NbSe_2$ (mixed phase), respectively, obtained along the [1$\bar{1}$00] direction of the silicon carbide (SiC) substrate. The top panels illustrate the sample and the substrate. (**d**) Constant-current STM image of a surface area of 100×50 nm (sample bias voltage $V_s=-1.0$ V and set-point tunneling current $I_t=100$ pA). (**e**) Height profile along a cut indicated by yellow lines in **d**. (**f**, **g**) High-resolution STM images measured in the surface region enclosed by the rectangle in **d** for type-A ($V_s=-0.5$ V) and type-B ($V_s=+0.6$ V) islands, respectively. (**h**) Representative tunneling spectra for type-A (red) and type-B (blue) islands.

samples was calibrated with a gold film deposited onto the substrate. First-principles band-structure calculations for free-standing 2*H*- and 1*T*-$NbSe_2$ monolayers were carried out by using the Quantum Espresso code.[25] Spin–orbit interactions were included in the calculations. The plane-wave cutoff energy and the *k*-point mesh were set to be 30 Ry and 12×12×1, respectively. The thickness of the inserted vacuum layer in a model crystal was set to ~10 Å.

RESULTS AND DISCUSSION

We used the van der Waals epitaxy technique[26] to fabricate monolayer $NbSe_2$ (Ugeda *et al.*[13]) by using bilayer graphene grown on silicon carbide as a substrate. Figure 1b shows the reflection high-energy electron diffraction pattern of bilayer graphene on 6*H*-SiC(0001), which signified a 1×1 streak pattern and $6\sqrt{3}\times6\sqrt{3}R30^\circ$ spots originating from the bilayer graphene and the buffer layer beneath it, respectively.[23,24] After co-evaporation of Nb and Se atoms onto a substrate kept at 530 °C in ultrahigh vacuum, the reflection high-energy electron diffraction intensity of $6\sqrt{3}\times6\sqrt{3}R30^\circ$ spots was reduced and a new 1×1 pattern appeared (Figure 1c). This behavior is characteristic of a TMD ultrathin film, as has been observed in monolayer WSe_2 and $TiSe_2$ on bilayer graphene.[23,24] STM revealed the formation of monolayer $NbSe_2$ islands (Figure 1d), whose height (~ 0.7 nm; see line profile in Figure 1e) was nearly equal to the distance between adjacent $NbSe_2$ layers in bulk 2*H*-$NbSe_2$, 0.63 Å.[10] We found that this film was composed of two different types of islands. One, called type-A here, exhibited a 1×1 atomic structure (Figure 1f), whereas the other, type-B, showed no clear atomic order. The former islands showed characteristic V-shaped density of states with a finite density of states at zero-bias voltage in the *dI*/*dV* curve at $T=6$ K, a result reminiscent of the spectral features of bulk 2*H*-$NbSe_2$.[18] This island type is probably made of 2*H* domains. However, the *dI*/*dV* curve of type-B islands showed markedly different characteristics; the density of states vanished in a wide energy region of ±0.2 eV with respect to E_F, indicating an insulating nature with an energy gap of ~0.4 eV. These results demonstrated that both metallic and insulating crystal phases coexisted in this monolayer $NbSe_2$ film.

To further clarify the nature of the two different islands, we performed ARPES on this film. It was expected that the characteristic spectral features from both domains would be simultaneously observed in an ARPES spectrum, because this technique probes a relatively large surface area (~2×2 mm^2). As shown in Figure 2a, the ARPES-intensity plot along the ΓM cut resolved several dispersive bands in the valence band region, reflecting the high single-crystallinity of the film. Figure 2b shows the valence-band ARPES-intensity plot of bulk 2*H*-$NbSe_2$, which is useful for distinguishing the contribution of the 2*H* phase in a monolayer film, because the overall experimental valence band dispersion in this wide energy range is known to be similar between the bulk and the monolayer.[13,15,16] In previous studies, the band calculations have revealed several differences in the band dispersions near E_F between the bulk and the monolayer, such as the presence or absence of the k_z dispersion in the Nb 4*d* band and the E_F crossing or non-crossing of the anti-bonding Se p_z band.[13,27] A side-by-side comparison of the ARPES-intensity plots in Figure 2a and b revealed that the observed band structures shared several common features, for example, the band near E_F around the M point, which crosses E_F midway between Γ and *M*, and the hole-like bands with the top of the dispersion at the binding energies (E_B) of 0.9 and 1.2 eV at Γ, as highlighted by the blue dashed curves. In Figure 2c, some corresponding bands are visible in the calculated band structure for monolayer 2*H*-$NbSe_2$, whereas several quantitative differences are also apparent in the energy of the bands (see, for example, the hole-like bands at $E_B\sim1$ eV at Γ). In addition to the bands ascribed to the 2*H* phase, Figure 2a shows additional bands that are absent in bulk and monolayer

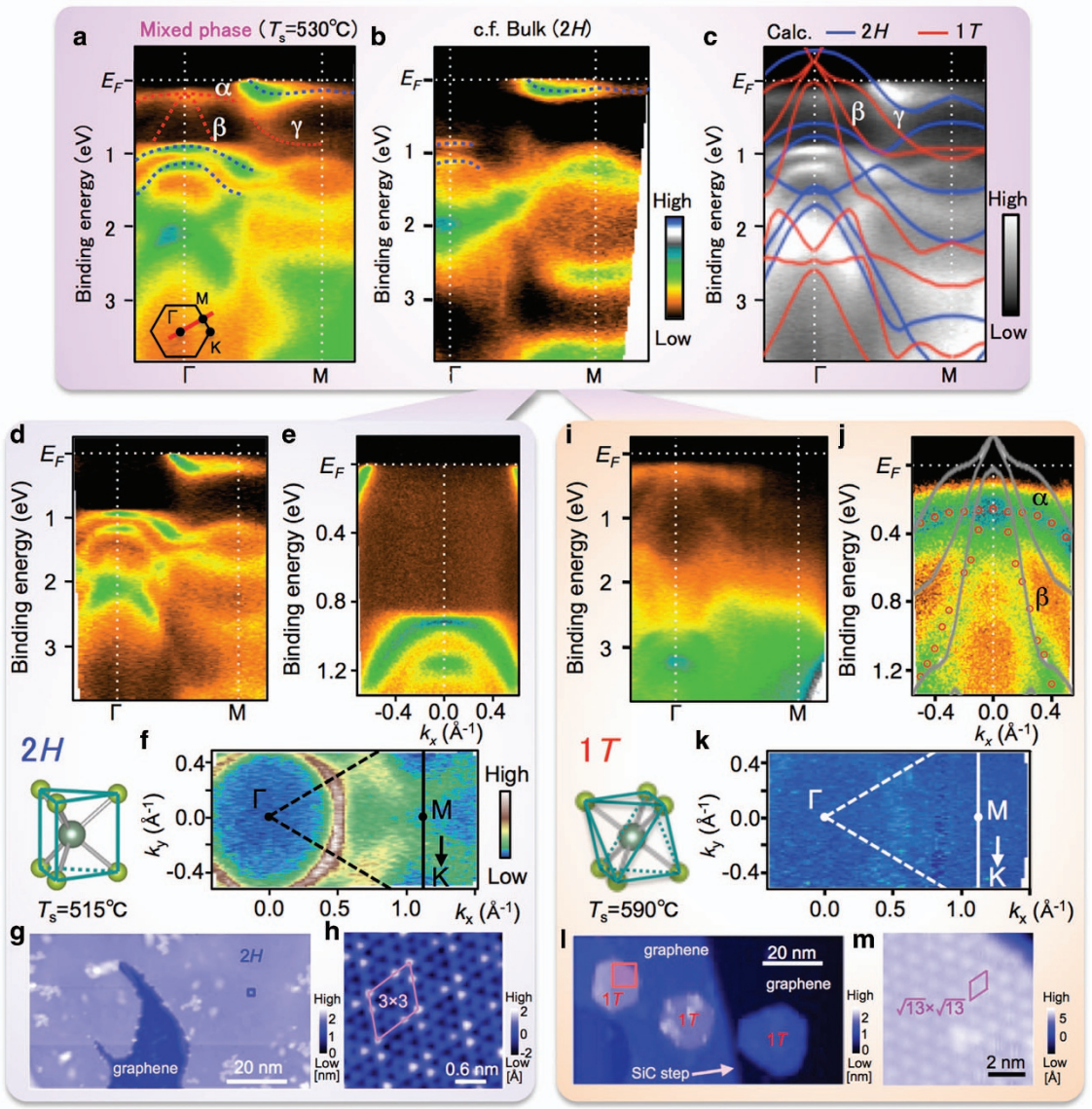

Figure 2 Electronic structure of monolayer 2*H*- and 1 *T*-$NbSe_2$. (**a**) Plot of valence-band ARPES intensity for monolayer $NbSe_2$ (mixed phase obtained at a substrate temperature T_S of 530 °C) measured along the Γ-M cut. ARPES data were recorded at T=40 K at the He-Iα line ($h\nu$=21.218 eV). (**b**) As in **a**, but for a cleaved surface of bulk 2*H*-$NbSe_2$. Blue dashed curves in **a**, **b** highlight the band dispersions that are commonly seen in **a**, **b**. Red dashed curves are a guide, indicating the bands that are absent in bulk 2*H*-$NbSe_2$. (**c**) Calculated band structure obtained from the first-principles band calculations for monolayer 2*H*- (blue) and 1 *T*- (red) $NbSe_2$ compared with the ARPES-intensity plot of monolayer $NbSe_2$ (mixed phase; as in **a**, but plotted in grayscale). (**d**, **e**) ARPES intensity plotted as a function of wavevector and binding energy for monolayer 2*H*-$NbSe_2$ (T_S=515 °C) in the valence band and near-E_F regions, respectively. (**f**) ARPES-intensity mapping at E_F plotted as a function of the two-dimensional wavevector for monolayer 2*H*-$NbSe_2$. The intensity at E_F was obtained by integrating the ARPES intensity within ±10 meV of E_F. The solid and dashed lines indicate the high-symmetry lines in the Brillouin zone for the (1×1) structure. (**g**) Constant-current STM image for monolayer 2*H*-$NbSe_2$ (sample bias voltage V_S=500 mV) measured at 4 K. (**h**) STM image expanded in the area enclosed by the small rectangle in **g** (V_S=10 mV). The diamond corresponds to the 3×3 unit cell. (**i**–**m**) As in **d**–**h** but for monolayer 1*T*-$NbSe_2$ (T_S=590 °C). The sample bias-voltage in **l**, **m** is V_S=−2 V. The diamond in **m** corresponds to the $\sqrt{13}\times\sqrt{13}$ unit cell arising from the star-of-David clusters.

2*H*-$NbSe_2$,[13,15,16] such as a relatively flat feature at E_B—0.4 eV around Γ (here denoted the α-band), a faint hole-like band at Γ (β-band) and a larger hole-like band (γ-band), as highlighted by the red dashed curves. These bands are likely to be of 1*T* phase in origin, because a corresponding feature in the calculated bands for monolayer 1*T*-$NbSe_2$ (Figure 2c) is apparent, particularly in the β- and γ-bands. Intriguingly, although the calculations predict the E_F crossings of hole-like bands around Γ, the ARPES intensity was strongly suppressed around E_F, thus suggesting an opening of an energy gap. Apparently, this gap was not an ordinary band gap, because the first-principles calculation failed to reproduce it, as shown in Figure 2j, which highlights the essential difference between the experimental and the calculated band dispersions around E_F. The opening of such an energy gap could not be explained in terms of carrier doping, because the band calculation for monolayer 1*T*-$NbSe_2$ showed no band gap around the Γ point, irrespective of the location of the chemical potential (Figure 2c). Instead, the observed gap may have arisen from a Mott–Hubbard gap, because the similar material bulk 1*T*-$TaSe_2$ shows almost identical band dispersions in the Mott phase.[28–30] In this context, the α-band was assigned to the lower Hubbard band.

Moreover, the insulating type-B islands in the STM image probably arose from the 1*T* phase, taking into account the similar energy scales for the gap below E_F found by ARPES and STM (~0.25 eV), as seen from a comparison of Figures 1h and 2j.

Having established the existence of a 1*T*/2*H*-mixed phase in monolayer $NbSe_2$, we next addressed how to selectively fabricate these two phases. We found that the temperature of the bilayer graphene substrate (T_S) during the epitaxy of the $NbSe_2$ film was a major parameter controlling the crystal phase. Whereas the mixed phase presented in Figures 1 and 2a was obtained at $T_S = 530$ °C, we found that the 2*H* (1*T*) single phase was obtained at a slightly lower (higher) T_S. As evident from Figure 2d and e, which show the ARPES intensities for the 2*H* phase ($T_S = 515$ °C), no obvious mixture of the 1*T*-phase bands was observed (compared with Figure 2a and d). Similarly, the ARPES intensity for the 1*T* phase ($T_S = 590$ °C) showed negligible contamination from the 2*H* phase, as evident from the absence of E_F crossing bands, as shown in Figure 2i and j. This selective fabrication of the 2*H* and 1*T* phases is also highlighted in Figure 2f and k, which show that the Fermi surface (FS) of the 2*H* phase consisted of a large hexagonal pocket at Γ and another large pocket at K (Figure 2f), as in the bulk sample,[15,16] whereas the FS was completely absent in the 1*T* phase, as seen from the featureless intensity pattern at E_F (Figure 2k). The control of crystal phases via temperature has been used in the chemical vapor transport method to obtain 1*T* and 2*H* phases in some bulk TMDs.[31–33] Our results thus suggest that temperature control is a key factor for obtaining different crystal phases in both monolayer and bulk TMDs.

The selective fabrication of 1*T* and 2*H* phases was further corroborated by our STM measurements. We found that the 1*T* phase ($T_s = 590$ °C) consisted of several monolayer 1*T* islands on the graphene substrate (Figure 2l), unlike the 2*H* counterpart, which appeared to grow layer by layer, as inferred from its large terrace size (Figure 2g). Intriguingly, closer examination of one of the 1*T* islands in Figure 2m revealed the modulation of density of states with $\sqrt{13} \times \sqrt{13}$ periodicity (note that this modulation is not clearly resolved in the 1*T*/2*H*-mixed phase in Figure 1g, probably because of the low film quality). This result strongly suggests the formation of 'star-of-David' clusters, similar to the case of the Mott-insulating (commensurate CDW) phases of bulk 1*T*-TaS_2 and $TaSe_2$,[28,30,34] thus supporting the Mott-insulating nature of the 1*T* phase. In contrast, the STM image of the 2*H* counterpart showed a 3×3 intensity modulation (Figure 2h), which followed the periodicity of the CDW in bulk and monolayer 2*H*-$NbSe_2$.[13,26] These STM results, together with the ARPES results, firmly establish the intrinsic differences between the electronic states of the 1*T* and 2*H* phases.

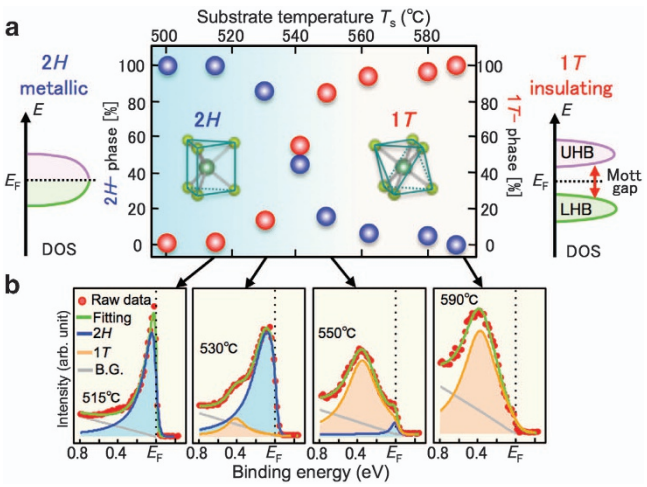

Figure 3 How to selectively fabricate monolayer 2*H*- and 1*T*-$NbSe_2$. (**a**) Surface area ratio between the 2*H* and 1*T* domains, plotted as a function of T_S, obtained by numerical fits to energy distribution curves (EDCs). The left and right panels illustrate the schematic density of states (DOS) for monolayer 2*H*- and 1*T*-$NbSe_2$, respectively. (**b**) Near-E_F EDC at $k_x = 0.5$ Å^{-1} for monolayer $NbSe_2$ films fabricated at various substrate temperatures ($T_S = 515$, 530, 560 and 590 °C). The green curves are the numerical fittings with two Lorentzian curves (representing the 1*T* (red) and 2*H* (blue) domains) and a linearly decreasing background multiplied by the Fermi–Dirac distribution function. The ratio between the 2*H* and 1*T* phases was estimated according to the total spectral weight of the Lorentzians.

To experimentally determine the temperature ranges suitable for the selective growth of pure 1*T* or 2*H* single phases, we performed systematic ARPES measurements for samples with various T_S values. We evaluated the ratio of 1*T* and 2*H* components from the energy distribution curve along the ΓM cut on the hexagonal pocket, seen in the 2*H* phase ($k_x = 0.5$ Å^{-1}). We numerically fit the energy distribution curve with two Lorentzian peaks originating from the 2*H* and 1*T* phases located at around 0 and 0.4 eV, respectively. In Figure 3b, the energy distribution curve for $T_S = 515$ °C showed a single peak at E_F, thus supporting its purely 2*H*-phase nature. On increasing T_S, the intensity of this peak was monotonically reduced, in accordance with the evolution of the 0.4 eV peak. This finding suggested that the ratio between the 1*T* and 2*H* phases systematically changes as a function of T_S, as highlighted by the phase diagram in Figure 3a. We also found that T_S values below 500 °C or above 600 °C were not suitable for the fabrication of monolayer $NbSe_2$, owing to the presence of multiple 2*H* domains with unfixed axis orientations and/or the difficulty of maintaining a stable monolayer crystal phase. From this empirical evidence, together with the results of Figure 3a, we concluded that the T_S values best suited for obtaining 2*H* or 1*T* single phases are 500–515 °C and 580–600 °C, respectively.

A previous study of monolayer 2*H*-$NbSe_2$ (Ugeda *et al.*[13]) has suggested that two types of 2*H* domains, rotated by 30° with respect to each other, can exist when the film is fabricated at low T_S (~330 °C). As described above, we found a way to selectively fabricate the single-domain 2*H* phase by keeping the T_S above 500 °C. When two domains are mixed in a sample, the appearance of a complicated FS is expected. For example, besides the intrinsic FS at K, a replica FS should appear around M. In contrast, as shown in Figure 2d, our ARPES intensity mapping for the $T_s = 515$ °C sample showed no signature of the FS at M, thereby strongly suggesting the single-domain nature of our 2*H*-phase sample. This conclusion is also supported by the experimental evidence that the FS at the Γ point exhibited a clear hexagonal shape consistent with the sixfold symmetry of a single domain.

The present success of the selective fabrication of insulating 1*T* and metallic 2*H* phases may contribute to realizing a field effect transistor based on semiconducting monolayer 1*T*-$NbSe_2$ and metallic 2*H*-$NbSe_2$. Although polymorph field effect transistors have recently been reported by using other TMDs such as MoS_2 and $MoTe_2$,[8,9] the unique Mott-insulating state of 1*T*-$NbSe_2$, distinct from the states of the band-insulating 2*H*-MoS_2 and 2*H*-$MoTe_2$, would provide a new means of controlling a device, because the characteristics of the Mott-insulating state in the 1*T* phase are known to be altered by various physical parameters, such as pressure and disorder.[34,35] Furthermore, as monolayer 2*H*-$NbSe_2$ exhibits superconductivity robust against magnetic fields owing to space inversion symmetry breaking and the resultant spin imbalance in the electronic states,[12] the present result also opens a path toward atomic-layer electronics based on superconductor/semiconductor heterojunctions.

CONFLICT OF INTEREST

The authors declare no conflict of interest.

ACKNOWLEDGEMENTS

We thank K Yamada, H Kimizuka, N Shimamura, Y Tanaka and S Souma for their help with the ARPES experiments. We also thank T Koretsune for help with using the quantum ESPRESSO package. This work was supported by the JSPS KAKENHI Grant Numbers JP15H02105, JP25107003 and JP15H05853, the Program for Key Interdisciplinary Research and the World Premier International Research Center, Advanced Institute for Materials Research.

Author contributions: YN and KS carried out the fabrication of thin films, their characterization and the ARPES measurements. KU fabricated the bulk 2*H*-$NbSe_2$ single crystals. KS performed the band calculations. RS, YO, PH and TH performed the STM experiments. YN, KS, TS and TT finalized the manuscript with input from all the authors.

1 Novoselov, K. S., Geim, A. K., Morozov, S. V., Jiang, D., Katsnelson, M. I., Grigorieva, I. V., Dubonos, S. V. & Firsov, A. A. Two-dimensional gas of massless Dirac fermions in graphene. *Nature* **438**, 197–200 (2005).
2 Wang, Q.-Y., Li, Z., Zhang, W.-H., Zhang, Z.-C., Zhang, J.-S., Li, W., Ding, H., Ou, Y.-B., Deng, P., Chang, K., Wen, J., Song, C.-L., He, K., Jia, J.-F., Ji, S.-H., Wang, Y.-Y., Wang, L.-L., Chen, X., Ma, X.-C. & Xue, Q.-K. Interface-induced high-temperature superconductivity in single unit-cell FeSe films on $SrTiO_3$. *Chin. Phys. Lett.* **29**, 037402 (2012).
3 Mermin, N. D. Crystalline order in two dimensions. *Phys. Rev.* **176**, 250–254 (1968).
4 Py, M. A. & Haering, R. R. Structural destabilization induced by lithium intercalation in MoS_2 and related compounds. *Can. J. Phys.* **61**, 76–84 (1983).
5 Kang, Y., Najmaei, S., Liu, Z., Bao, Y., Wang, Y., Zhu, X., Halas, N. J., Nordlander, P., Ajayan, P. M., Lou, J. & Fang, Z. Plasmonic hot electron induced structural phase transition in a MoS_2 monolayer. *Adv. Mater.* **26**, 6467–6471 (2014).
6 Lin, Y.-C., Dumcenco, D. O., Huang, Y.-S. & Suenaga, K. Atomic mechanism of the semiconducting-to-metallic phase transition in single-layered MoS_2. *Nat. Nanotechnol.* **9**, 391–396 (2014).
7 Ambrosi, A., Sofer, Z. & Pumera, M. 2H → 1 T phase transition and hydrogen evolution activity of MoS_2, $MoSe_2$, WS_2 and WSe_2 strongly depends on the MX_2 composition. *Chem. Commun.* **51**, 8450–8453 (2015).
8 Kappera, R., Voiry, D., Yalcin, S. E., Branch, B., Gupta, G., Mohite, A. D. & Chhowalla, M. Phase-engineered low-resistance contacts for ultrathin MoS_2 transistors. *Nat. Mater.* **13**, 1128–1134 (2014).
9 Cho, S., Kim, S., Kim, J. H., Zhao, J., Seok, J. D., Keum, H., Baik, J., Choe, D.-H., Chang, K. J., Suenaga, K., Kim, S. W., Lee, Y. H. & Yang, H. Phase patterning for ohmic homojunction contact in $MoTe_2$. *Science* **349**, 625–628 (2015).
10 Wilson, J. A., Di Salvo, F. J. & Mahajan, S. Charge-density waves and superlattices in the metallic layered transition metal dichalcogenides. *Adv. Phys.* **24**, 117–201 (1975).
11 Xi, X., Zhao, L., Wang, Z., Berger, H., Forró, L., Shan, J. & Mak., K. F. Strongly enhanced charge-density-wave order in monolayer $NbSe_2$. *Nat. Nanotechnol.* **10**, 765–769 (2015).
12 Xi, X., Wang, Z., Zhao, W., Park, J.-H., Law, K. T., Berger, H., Forró, L., Shan, J. & Mak., K. F. Ising pairing in superconducting $NbSe_2$ atomic layers. *Nat. Phys.* **12**, 139–143 (2016).
13 Ugeda, M. M., Bradley, A. J., Zhang, Y., Onishi, S., Chen, Y., Ruan, W., Ojeda-Aristizabal, C., Ryu, H., Edmonds, M. T., Tsai, H.-Z., Riss, A., Mo, S.-K., Lee, D., Zettl, A., Hussain, Z., Shen, Z.-X. & Crommie, M. F. Characterization of collective ground states in single-layer $NbSe_2$. *Nat. Phys.* **12**, 92–97 (2016).
14 Cao, Y., Mishchenko, A., Yu, G. L., Khestanova, E., Rooney, A. P., Prestat, E., Kretinin, A. V., Blake, P., Shalom, M. B., Woods, C., Chapman, J., Balakrishnan, G., Grigorieva, I. V., Novoselov, K. S., Piot, B. A., Potemski, M., Watanabe, K., Taniguchi, T., Haigh, S. J., Geim, A. K. & Gorbachev, R. V. Quality heterostructures from two-dimensional crystals unstable in air by their assembly in inert atmosphere. *Nano Lett.* **15**, 4914–4921 (2015).
15 Yokoya, T., Kiss, T., Chainani, A., Shin, S., Nohara, M. & Takagi, H. Fermi surface sheet-dependent superconductivity in 2*H*-$NbSe_2$. *Science* **294**, 2518–2520 (2001).
16 Rahn, D. J., Hellmann, S., Kalläne, M., Sohrt, C., Kim, T. K., Kipp, L. & Rossnagel, K. Gaps and kinks in the electronic structure of the superconductor 2*H*-$NbSe_2$ from angle-resolved photoemission at 1 K. *Phys. Rev. B* **85**, 224532 (2012).
17 Ramšak, N., van Midden, H. J. P., Prodan, A., Marinković, V., Boswell, F. W. & Bennett, J. C. Defect-induced room-temperature modulation in $NbSe_2$. *Phys. Rev. B* **60**, 4513–4516 (1999).
18 Komori, F., Iwaki, T., Hattori, K., Shiino, O. & Hasegawa, T. New superstructure on the surface of 2*H*-$NbSe_2$ and tunneling spectra at 4.2 K. *J. Phys. Soc. Jpn* **66**, 298–301 (1997).
19 Wang, H., Lee, J., Dreyer, M. & Barker, B. I. A scanning tunneling microscopy study of a new superstructure around defects created by tip–sample interaction on 2*H*-$NbSe_2$. *J. Phys. Condens. Matter* **21**, 265005 (2009).
20 Kadijk, F. & Jellinek, F. On the polymorphism of niobium diselenide. *J. Less Common. Met.* **23**, 437–441 (1971).
21 Koslowski, B., Xu, W., Blackford, B. & Jericho, M. H. Observation of a superlattice in silver-intercalated $NbSe_2$ by scanning tunneling microscopy. *Phys. Rev. B* **54**, 11706–11709 (1996).
22 Di Salvo, F. J., Wilson, J. A., Bagley, B. G. & Waszczak, J. V. Effects of doping on charge-density waves in layer compounds. *Phys. Rev. B* **12**, 2220–2236 (1975).
23 Sugawara, K., Sato, T., Tanaka, Y., Souma, S. & Takahashi., T. Spin- and valley- coupled electronic states in monolayer WSe_2 on bilayer graphene. *Appl. Phys. Lett.* **107**, 071601 (2015).
24 Sugawara, K., Nakata, Y., Shimizu, R., Patrick, H., Hitosugi, T., Sato, T. & Takahashi, T. Unconventional charge-density-wave transition in monolayer 1 *T*-$TiSe_2$. *ACS Nano* **10**, 1341–1345 (2016).
25 Giannozzi, P., Baroni, S., Bonini, N., Calandra, M., Car, R., Cavazzoni, C., Ceresoli, D., Chiarotti, G. L., Cococcioni, M., Dabo, I., Corso, A. D., de Gironcoli, S., Fabris, S., Fratesi, G., Gebauer, R., Gerstmann, U., Gougoussis, C., Kokalj, A., Lazzeri, M., Martin-Samos, L., Marzari, N., Mauri, F., Mazzarello, R., Paolini, S., Pasquarello, A., Paulatto, L., Sbraccia, C., Scandolo, S., Sclauzero, G., Seitsonen, A. P., Smogunov, A., Umari, P. & Wentzcovitch, R. M. QUANTUM ESPRESSO: a modular and open-source software project for quantum simulations of materials. *J. Phys. Condens. Matter* **21**, 395502 (2009).
26 Koma, A., Sunouchi, K. & Miyajima, T. Fabrication and characterization of heterostructures with subnanometer thickness. *Microelectron. Eng.* **2**, 129–136 (1984).
27 Calandra, M., Mazin, I. I. & Mauri, F. Effect of dimensionality on the charge-density wave in few-layer 2*H*-$NbSe_2$. *Phys. Rev. B* **80**, 241108(R) (2009).
28 Ang, R., Tanaka, Y., Ieki, E., Nakayama, K., Sato, T. L., Li, J., Lu, W. J., Sun, Y. P. & Takahashi, T. Real-space coexistence of the melted Mott state and superconductivity in Fe-substituted 1 *T*-TaS_2. *Phys. Rev. Lett.* **109**, 176403 (2012).
29 Perfetti, L., Georges, A., Florens, S., Biermann, S., Mitrovic, S., Berger, H., Tomm, Y., Höchst, H. & Grioni, M. Spectroscopic signatures of a bandwidth-controlled Mott transition at the surface of 1 *T*-$TaSe_2$. *Phys. Rev. Lett.* **90**, 166401 (2003).
30 Colonna, S., Ronci, F., Cricenti, A., Perfetti, L., Berger, H. & Grioni, M. Mott phase at the surface of 1 *T*-$TaSe_2$ observed by scanning tunneling microscopy. *Phys. Rev. Lett.* **94**, 036405 (2005).
31 Samnakay, R., Wickramaratne, D., Pope, T. R., Lake, R. K., Salguero, T. T. & Balandin, A. A. Zone-folded phonons and the commensurate–incommensurate charge-density-wave transition in 1 *T*-$TaSe_2$ thin films. *Nano Lett.* **15**, 2965–2973 (2015).
32 Renteria, J., Samnakay, R., Jiang, C., Pope, T. R., Goli, P., Yan, Z., Wickramaratne, D., Salguero, T. T., Khitun, A. G., Lake, R. K. & Balandin, A. A. All-metallic electrically gated 2H-$TaSe_2$ thin-film switches and logic circuits. *J. Appl. Phys.* **115**, 034305 (2014).
33 Yan, Z., Jiang, C., Pope, T. R., Tsang, C. F., Stickney, J. L., Goli, P., Renteria, J., Salguero, T. T. & Balandin, A. A. Phonon and thermal properties of exfoliated $TaSe_2$ thin films. *J. Appl. Phys.* **114**, 204301 (2013).
34 Sipos, B., Kusmartseva, A. F., Akrap, A., Berger, H., Forró, L. & Tutiš, E. From Mott state to superconductivity in 1 *T*-TaS_2. *Nat. Mater.* **7**, 960–965 (2008).
35 Xu, P., Piatek, J. O., Lin, P.-H., Sipos, B., Berger, H., Forró, L., Rønnow, H. M. & Grioni, M. Superconducting phase in the layered dichalcogenide 1 *T*-TaS_2 upon inhibition of the metal-insulator transition. *Phys. Rev. B* **81**, 172503 (2010).